# Measurement of band offsets and shunt resistance in CdTe solar cells through temperature and intensity dependence of open circuit voltage and photoluminescence

Craig H. Swartz[a,*], Sadia R. Rab[a], Sanjoy Paul[b], Maikel F.A.M. van Hest[c], Benjia Dou[c], Joseph M. Luther[c], Gregory F. Pach[c], Corey R. Grice[d], Dengbing Li[d], Sandip S. Bista[d], Elizabeth G. LeBlanc[a], Matthew O. Reese[c], Mark W. Holtz[b], Thomas H. Myers[a], Yanfa Yan[d], and Jian V. Li[a]

[a] Materials Science, Engineering, and Commercialization Program, Texas State University, 601 University Dr., San Marcos, Texas, 78666 U.S.A.

[b] Department of Physics, Texas State University, 601 University Dr., San Marcos, Texas, 78666 U.S.A.

[c] National Renewable Energy Laboratory, 15013 Denver West Parkway, Golden, Colorado, 80401 U.S.A.

[d] Department of Physics and Astronomy, The University of Toledo, McMaster Hall, Room 2017, Toledo, Ohio 43606 U.S.A.

Band offsets at the back contact and front window layer in CdTe-based solar cells affect photovoltaic performance and challenge standard characterization methods. By analyzing the temperature and excitation dependence of both open circuit voltage and absolute photoluminescence intensity, we show that the effects band offsets can be separated from the effects of recombination and shunting. Solar cells were grown with MgZnO window layers and compared to cells with CdS window layers containing varying amounts of oxygen. It was demonstrated that band alignment rather than reduced recombination velocity is the reason for the success of MgZnO as a front interface contact. An assortment of thin back contact interlayers were also deposited, and a PbTe interlayer showed some promise as an Ohmic contact to the CdTe, though it appears to induce a photoconductive shunt. Finally, we show that the shunting resistance given by a standard current-voltage curve technique generally does not represent a physically meaningful quantity unless it is well below one kiloOhm square cm.

Keywords: Photovoltaic device characterization; Loss analysis; Model fitting; Contact barrier; Recombination; Injection dependence

## 1. Introduction

The achievement of an ohmic back contact has been elusive in CdTe-based solar cells. The ubiquitous back-contact barrier, of height $\Phi_b$, is a challenge for standard characterization methods and for further improving photovoltaic performance. The back-contact barrier decreases the fill factor and open circuit voltage ($V_{OC}$) in complicated ways, (Pan et al., 2006) and distorts capacitance-voltage (C-V) measurements of the doping concentration. (Li et al., 2012) When measuring trapping center properties by capacitance-frequency (admittance spectroscopy, or AS) technique, trap signatures can be altered by the presence of $\Phi_b$ (Marin et al., 2013) and apparent signatures can be wholly produced. (Li et al., 2010) It has been questioned whether $\Phi_b$ may

* Corresponding author.
E-mail address: craig.swartz@txstate.edu

render admittance spectroscopy unusable for its original purpose of characterizing deep centers. (Lauwaert et al., 2013)

A reduced $\Phi_b$ is generally desirable for the back contact. While metals with deep work functions are more likely to be successful for contact to *p*-type materials, other factors at the back interface have considerable influence as well. For example, it has been found that a Te-rich back surface tends to result in improved performance. It is possible that a thin layer with a favorable conduction band offset from CdTe may be formed from Cu-Te compounds, (Jaegermann et al., 2009; Wang et al., 2017) and that such a layer would have an electron blocking effect. Alternatively, the Te may itself form an intermediate band offset between the absorber and back contact. (Song et al., 2018) Another possible mechanism is that the Te may block Cu from diffusing into the CdTe absorber and reaching the front buffer layer, (Xia et al., 2014) where excessive Cu becomes deleterious. (Korevaar et al., 2011)

Other factors at the back contact include the use of interlayers in an attempt to lessen the shunt conductance ($G_{SH}$) between the front and back electrodes.(Major et al., 2017; Tessema and Giolando, 2012) Even without a true pinhole contact, any sufficiently thin region within the absorber can exhibit space-charge-limited current (SCLC), where the conductance is approximately proportional to voltage $V$ with a proportionality constant $K$, or $G_{SH} \approx K\,V$. (Dongaonkar et al., 2010)

In addition to shunt conduction, various band offsets that may affect solar cell performance are shown in Fig. 1. In this diagram, a 4-µm thick *p*-CdTe absorber layer is depicted with a band gap of $E_G$ = 1.5 eV and a 90-nm thick buffer of CdS having a band gap of $E_{GW}$ = 2.5 eV. The front absorber-buffer junction conduction band offset ($\Delta E_C$), and the (hole-blocking) front valence band offset can be expressed in terms of $\Delta E_C$ and the band gaps as shown. The barrier height of the main junction is $\Phi_f$.

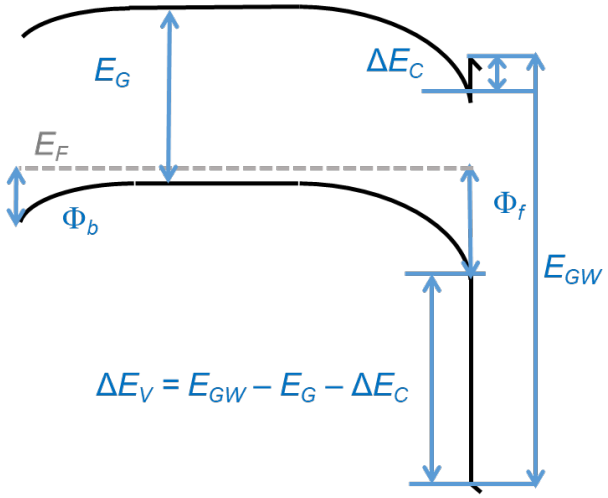


Fig. 1. Band offsets that may affect solar cell performance. A 4 µm thick *p*-type absorber layer is depicted with a band gap of $E_G$ = 1.5 eV and a 90 nm thick buffer having a band gap of $E_{GW}$ = 2.5 eV.

In this study, a number of interlayers are deposited at the back contact-absorber interface in an attempt to improve the back-contact properties of the solar cells. To correlate device properties such as band offsets and shunt with experimentally obtainable characteristics, we employ a measurement and analysis technique coupling the temperature and excitation dependence of $V_{OC}$ and photoluminescence intensity (PL-I) with numerical simulation studies.

A potentially overwhelming number of methods exist for correlating device properties to experimental current-voltage (JV) results. (Chan et al., 1986; Jordehi, 2016; Khan et al., 2011) These techniques are somewhat limited in their ability to provide physical insight, since, *e.g.*, the proportion of interfacial versus bulk recombination has no clear relationship with the contribution of each diode in a two-diode lumped-parameter circuit model. Additionally, the existence of a back-contact band offset is not generally considered in these models.

In recent years, temperature-dependent $V_{OC}$ has been used to probe recombination characteristics (Li et al., 2014) while avoiding the complexities of series resistance. (Hegedus and Shafarman, 2004; Turek, 2014) In that method, the $V_{OC}$ versus temperature relationship near room temperature is extrapolated to absolute zero. The extrapolated voltage value ($qE_a$) can be correlated with the location of recombination within the device. More recently, it has been found that the value of $qE_a$ can change with excitation, and this may be affected by front junction band offsets. (Brandt et al., 2017)

This study has the goal of extracting a set of solar cell parameters from multiple measurement types. In addition to the $V_{OC}$ and PL-I, we adopt the value of $\Phi_b$ from the rollover method on the current-voltage-temperature (JVT) curves. (Koishiyev et al., 2008) Only a few studies have aimed to combine multiple measurement types. (Mangan et al., 2015; Richter et al., 2015; Schoneberg et al., 2018; Sun et al., 2016) The effort presented here differs from these others in several important ways. First, series resistance complications are avoided, since although the rollover portion of the JV curve is in the forward current region, the rollover method should be robust against the effects of varying series resistance. (Demtsu et al., 2006) Second, rather than revising a model for each measurement technique to account for each new experimental feature qualitatively, the most suitable parameters are determined *quantitatively* by arriving at the least square error fit to the temperature- and excitation-dependent $V_{OC}$ data, and simultaneously to the PL-I data. To define a single rms difference between data and model for both open circuit voltage and PL-I, the PL-I data must be converted to units of eV. Therefore, the *absolute* PL intensity was measured, and the quasi-Fermi level splitting between the electron and hole populations ($\Delta E_F$) within the absorber was extracted from a calculation based on the Generalized Planck's Law. (Swartz et al., 2019)

Various back interlayers and front window layers are explored. The analysis shows that some interlayers were successful at reducing shunt conductance, but an interlayer was not found which reduced the barrier height without an accompanying increase in shunt resistance. The analysis also provided a way of obtaining the front window conduction band offset.

## 2. Experimental Details

Superstrate structures were fabricated beginning with three sequences of front buffer layers. The first sequence began with 2.3 mm thick AF45 borosilicate glass coated with bilayers of fluorine-doped tin oxide $SnO_2$:F (FTO) with 500nm thickness and undoped $SnO_2$ (TO) with 100 nm thickness, grown at the National Renewable Energy Laboratory (NREL) in a low pressure chemical vapor deposition system at 550˚C. Tetramethytin (TMT) was the tin precursor and bromotrifluoromethane was the F dopant source in an oxygen-rich ambient. Then, CdS:O with a thickness of 80 nm was deposited by magnetron sputtering, in a 6% $O_2$ in Ar ambient at 5 mTorr deposition pressure without heating. This window will be labeled CdS:O[6]. CdTe was deposited by close space sublimation (CSS) at 600 °C, at 16 Torr in a 6.25% $O_2$ in He ambient. A $CdCl_2$ activation anneal was performed at 400 °C in dry air, followed by rinsing in methanol and drying with $N_2$ gas to remove extra $CdCl_2$ from the surface.

A blade-coated layer of CdTe nanoparticles (NP) in a pyridine solution was then added to reduce surface roughness, eliminate pinholes, and allow for the deposition of interlayers. (Details to be published later by S. Rab, *et. al.*) A second $CdCl_2$ activation anneal was carried out for the added NP material by dipping the samples into a solution of $CdCl_2$ in methanol with ~15 mg/mL concentration, heated at 60 ℃ for 15 s, rinsed with isopropanol, dried with a stream of $N_2$, placed on a 350 °C Al block for 20 s, then placed onto an Al block at room temperature for rapid cooling. Back contact Cu doping was done by submerging in a dilute 0.1mM solution of $CuCl_2$ and DI water for 2 min followed by rinsing in DI water and drying with $N_2$, followed by a 225 °C, 30 min anneal, then 150 °C for 1 hour. Various interlayers were grown on devices with NP. Spin-coated Spiro-MeOTAD (2,2′,7,7′-tetrakis(N,N-di-p-methoxyphenylamino)-9,9′-spirobifluorene) and EH44 (2,7-Di(N,N-dimethoxyphenylamino)-N-(2-ethylhexyl)carbazole) are organic hole transport materials used in perovskite solar cells. (Leijtens et al., 2016) Evaporated selenium and sputter coated indium tin oxide (ITO) are known to have deep work functions, particularly ITO with Cl and Au, which is often used to accomplish the formation of Ohmic contacts to *p*-type materials. (Guo et al., 2010; Helander et al., 2011b) SnTe interlayers and PbTe interlayers were grown by molecular beam epitaxy to a thickness of 250 nm and doped with Tl to a high *p*-type concentration of $10^{19}$ $cm^{-3}$ to mitigate the back contact barrier. (Lee et al., 2012) Finally, a 100 nm thick Au layer was deposited by thermal evaporation, forming 0.25 $cm^2$ area devices.

A second window sequence, grown at the University of Toledo, began with 3.2 mm thick TEC-15M commercial substrates, which consist of soda lime glass coated with $SiO_2$ to prevent sodium migration, then FTO with 500nm thickness and undoped TO with 100nm thickness. CdS:O was deposited by sputtering to a thickness of 80 nm with 1% $O_2$ in Ar ambient at 10 mTorr deposition pressure at 270 °C. This CdS:O[1] window layer was followed by CdTe grown by CSS at 660 °C, 50 Torr He ambient. A $CdCl_2$ activation anneal was performed at 400 °C in dry air, followed by rinsing in methanol and drying with $N_2$ gas to remove extra $CdCl_2$ from the surface. Cu doping was achieved by the evaporation of ~ 3 nm of Cu and 40 nm of Au, forming 0.09 $cm^2$ area devices, followed by a 30 min anneal at 200 °C.

A third window sequence was grown at the University of Toledo on 3.2 mm thick TEC-15M substrates. MgZnO (MZO) was deposited by sputtering without heating at 6 mTorr pressure.

CdTe on this layer was grown by CSS at 560 °C. A $CdCl_2$ activation anneal was performed at 400 °C in dry air, with the exception of a final MgZnO device where it took place at 420 °C in an O-free ambient (He gas). The $CdCl_2$ activation step was followed by rinsing in methanol and drying with $N_2$ gas to remove extra $CdCl_2$ from the surface. Back contact Cu doping was done by submerging in a dilute solution of $CuCl_2$ and DI water for 2 min followed by rinsing in DI water and drying with $N_2$, followed by a 225 °C, 30 min anneal. Finally, a 40 nm thick Au layer was deposited by thermal evaporation, forming 0.09 $cm^2$ area devices.

To measure power conversion efficiency (PCE) at room temperature, a class A solar simulator lamp was used. To measure temperature- and excitation-dependent open-circuit voltage, illumination was provided by a spectrally uniform laser-driven light source filtered from 400 to 850 nm, focused with achromatic lenses, controlled by neutral density filters, and measured with a power meter. Knowing the spectra for the power meter response, the source, and the filters allows us to convert measured power meter current to photons $cm^{-2}$ $s^{-1}$. Since AM1.5 illumination gives a flux of $1.7\times10^{17}$ photons $cm^{-2}$ $s^{-1}$, with energy greater than the 1.5 eV band gap of CdTe, that flux was considered 1 sun equivalent. The current-voltage-temperature-intensity (JVTI) measurements were performed with this illumination inside of a helium closed-cycle cryogenic system at Texas State University using a Keysight B2912A source measure unit.

AC measurements were made with a Keysight E4990A impedance analyzer. For C-V, DC bias was varied from -1.0 to 0.7 V. For AS, the frequency sweep was additionally varied from 1 kHz to 1 MHz and the AC modulation amplitude was 35 $mV_{rms}$.

To measure the temperature- and excitation-dependent PL-I, devices were illuminated with a 660 nm diode laser focused by a 6.5× objective lens into a microscopy cryostat. The spot diameter was found to be 120 μm using the knife edge method on a cleaved wafer. (Passlack et al., 1998) The laser power, controlled by neutral density filters, was measured with a NIST-traceable power meter to obtain the intensity.

The superstrate solar cell devices were illuminated through the glass, which had a thickness of $d$ = 2.3 or 3.2 mm. Therefore, after the cleaved wafer was removed, the focus point was lowered to the floor of the stage where the active device would rest, then also raised by $(1/1 - 1/n_g)d$ to account for the altered focus point of the laser light, where $n_g$ = 1.5 is the index of refraction of the glass.

The resulting PL was collected through the same objective and passed through filters to remove the laser light. The PL intensity was recorded by a photomultiplier (PMT) attached to a lock-in amplifier with the laser chopped at 400 Hz. The laser intensity could be changed by a series of calibrated neutral density filters. To relate the number of photons to a raw detector signal, we measured the signal from an excitation laser spot on a Spectralon reflectance standard. (Swartz et al., 2019)

Studies were conducted and analyzed varying the temperature from 200 to 350 K, since the properties below 200 K can be dominated by more detailed effects such as carrier freeze-out, band gap temperature dependence, and inhomogeneous barrier heights. (Fiat et al., 2012) $V_{OC}$ was analyzed up to 350 K to ensure resolution of its temperature dependence near room

temperature. (Li et al., 2014) The excitation range for PL-I was chosen to be high enough for all samples to have a strong signal-to-noise ratio and yet low enough for laser spot heating effects to be minor. (Sohal et al., 2018)

## 3. Analysis

The measurement of JVTI allowed the determination of $\Phi_b$ through the rollover effect. (Koishiyev et al., 2008) The measurements of temperature and intensity dependent $V_{OC}$ and PL-I allowed the extraction of a number of physical parameters: the conduction band offset $\Delta E_C$, the SCLC shunt constant $K = G_{SH}/V$, and the effective capture coefficient for recombination centers, both within the absorber $c_a = N_{ta}\sigma_a v_{th}$ and at the absorber-buffer interface $c_s = N_{ts}\sigma_s v_{th}$, where $N_{ta}$ is the density of recombination centers, $N_{ts}$ is the sheet density of recombination centers at the interface, $\sigma$ is the respective capture cross section, and $v_{th}$ is the carrier thermal velocity. $c_a$ is also the reciprocal of the minimum lifetime for a carrier type which could be caused by the absorber's recombination center, and $c_s$ is also the maximum recombination velocity which could be caused by the interface recombination center.

The mobilities, effective masses, and permittivity ε were taken from the commonly used baseline. (Gloeckler et al., 2003) The absorber doping density was $p = 1\times10^{14}$ cm$^{-3}$ from C-V measurements. Within the heavily doped $SnO_2$:F front contact, the $E_F$ is 3.8 eV above its valence band.(Helander et al., 2011a) Given a 2.7 eV valence band offset between CdTe and $SnO_2$, (Klein, 2015) the front contact barrier height ($\Phi_f$) was therefore taken as 1.1 eV.

Since injection-dependent measurements are being considered, we cannot assume low injection or a constant minority carrier lifetime, particularly with such low doping. We will however make the common simplifying assumptions that dominant recombination states must be within the mid-gap energy range and that the capture cross sections for electrons and holes are equal. (Böer, 2013 ; Grover et al., 2013) In this case the recombination rate at a given location, where the electron concentration is $n$ and the hole concentration is $p$, becomes $R = c_{a,s}\, np/(n+p)$. Each parameter set yielded the quantities $V_{OC}$ and $\Delta E_F$ through a numerical model solving the continuity and Poisson's equations. (Seidman and Choo, 1972) The parameter set was adjusted to find the minimum square difference fit to the temperature- and excitation-dependent $V_{OC}$ and PL-I data simultaneously, using a differential evolution algorithm. (Storn and Price, 1997)

## 4. Results

Examples of the effect each experimental variable has on $V_{OC}$ are shown in Fig. 2. The data are from what will be called the Control sample, listed first in Table I. The $V_{OC}$ is typically greatest at low temperatures and high intensities where it is limited by the difference in the built-in voltages of the front and back junctions. (Halverson et al., 2013; Ott et al., 2015) In Fig. 2 (a), the simulated effect of increasing non-radiative recombination in the absorber material ($c_a$) is shown, illustrating the uncertainty in the $c_a$ parameter as fit to the measured voltages. The increasing slope of open circuit voltage with temperature ($dV_{OC}/dT$) is consistent with an increasing activation energy $qE_a$. The activation energy method of evaluating recombination associates a higher $qE_a$ with more dominant bulk recombination, and so there is a qualitative

agreement with the method presented here. (Grover et al., 2013; Li et al., 2014) In Fig. 2 (b) an increased shunt causes the low intensity $V_{OC}$ to drop, though shunting is less important at high intensity. (Proctor and Nguyen, 2015) Fig. 2 (c) replots the lowest intensity points in Fig. 2 (a) in 2D for clarity.

In Fig. 3 (a), also from the Control sample, non-radiative recombination is shown to cause a drop in the PL intensity as well. Meanwhile, the PL-I corresponding to shunting in Fig. 3 (b) is unaffected, since it is taken experimentally at a high intensity where shunting is less important.

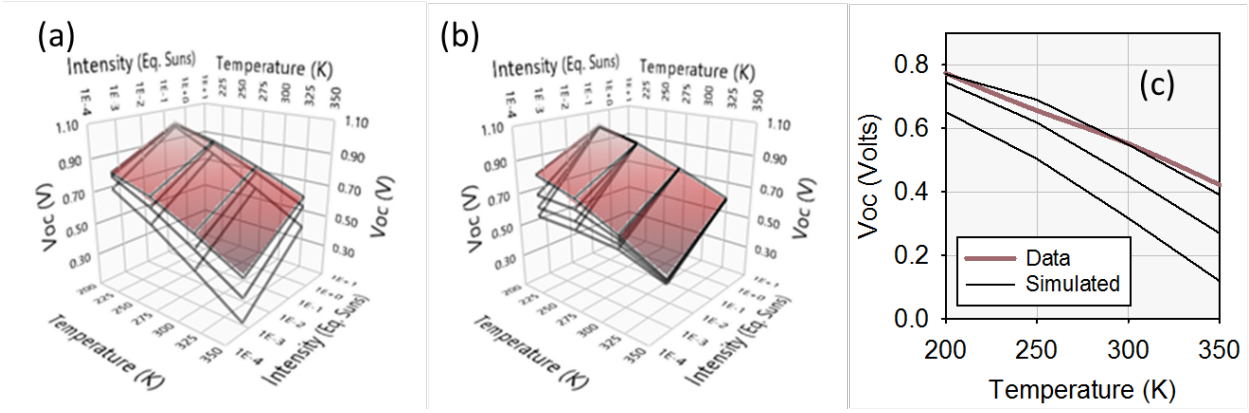


Fig. 2. $V_{OC}$ versus temperature and excitation intensity for the Control sample. $V_{OC}$ data is shown as a surface, and the grids are simulated $V_{OC}$ values, with parameters varying as: (a) $c_a$ is increased from 1.3 to 13 to 130 $\times 10^7$ $s^{-1}$, and as (b) the shunting constant $K$ is increased from 4 to 6 to 8 to 10 $\times 10^5$ $(\Omega\ V\ cm^2)^{-1}$. Each parameter increase (for both $c_a$ and $K$) corresponds to a grid with a lower $V_{OC}$. (c) Shows for clarity a cross section view of the lowest intensity points in (a).

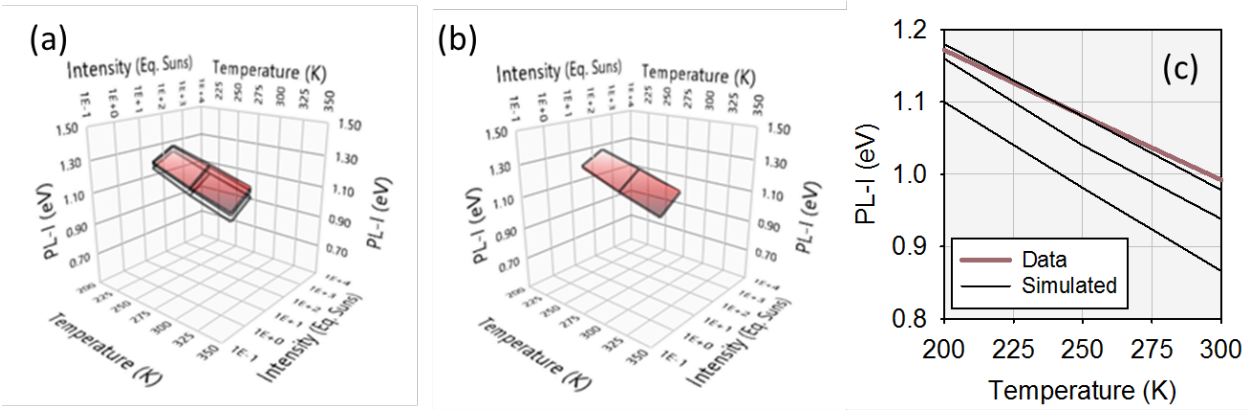


Fig. 3. PL-I converted to $\Delta E_F$ versus temperature and excitation intensity for the Control sample. Experimental PL-I data is drawn as a surface, and the grids are simulated PL-I values, with parameters varying as: (a) $c_a$ is increased from 1.3 to 13 to 130 $\times 10^7$ $s^{-1}$, and as (b) the shunting constant $K$ is increased from 4 to 6 to 8 to 10 $\times 10^5$ $(\Omega\ V\ cm^2)^{-1}$. Each parameter increase (for both $c_a$ and $K$) corresponds to a grid with a lower PL-I. (c) Shows a cross section view of the lowest intensity points in (a).

In addition to recombination within the absorber, interfacial recombination may be significant, and it is known to be compounded by a negative or cliff-like $\Delta E_C$. This is because such an offset can position a high *n*-type concentration in the buffer layer in close proximity to a high *p*-type concentration at the front edge of the absorber. (Song et al., 2016) Additionally, $\Delta E_C$ can directly affect the electrical properties, even without considering interfacial recombination. (Sozzi et al., 2014)

For the Control sample, introducing a negative or cliff-like $\Delta E_C$ had a weak effect on $V_{OC}$. This is because the interfacial recombination coefficient $c_s$ turned out to be fairly small. For illustration purposes, the result of a -0.1 eV cliff-like step in $\Delta E_C$ is shown in Fig. 4 (a) with an inflated $c_s$ (essentially an infinite surface recombination velocity at the CdTe-window interface) to make the effects of cliff-like offset more visible. In this case, the slope of $V_{OC}$ with temperature remains gentle with increasing interfacial recombination, in contrast to the case of increasing bulk recombination seen in Fig. 2 (a). This is again consistent with the method of evaluating recombination mechanisms by slopes, which associates a high intercept of the room temperature $V_{OC}$ slope, in the zero-temperature limit, with dominant bulk recombination. (Grover et al., 2013; Li et al., 2014)

A positive or spike-like $\Delta E_C$ results in an anomalous temperature peak of the $V_{OC}$, as in Fig. 4 (b). This spike-related maximum in the $V_{OC}$ (Schubbert et al., 2015) is more pronounced at high illumination, appearing between 250 and 300 K. The maximum can interfere with the standard method of probing recombination by finding $qE_a$ from room temperature $V_{OC}$. Here, it is being used to evaluate absorber-buffer band offsets by fitting $\Delta E_C$ to the $V_{OC}$ data.

Note that some of these quantities have overlapping effects on $V_{OC}$; for example the increased interfacial recombination shown in Fig. 4 (a) is most effective at suppressing the low temperature, low intensity $V_{OC}$. This is similar to the primary effect of shunt resistance shown in Fig. 2 (b). Therefore these two parameters can become difficult to resolve, particularly when other effects are present.

To remove ambiguity, the analysis of PL-I-T is helpful. Comparing Fig. 5 (a) to Fig. 3 (b), we see that the interfacial recombination has a deleterious effect on PL intensity while shunting has no effect. Thus, requiring agreement of the model outputs to both $V_{OC}$ and PL-I data distinguishes these cases. In general, $V_{OC}$ is controlled by both the rate of recombination and by band offsets, but the intensity of PL tends to be sensitive to recombination, not band offsets. (López Salas et al., 2017)

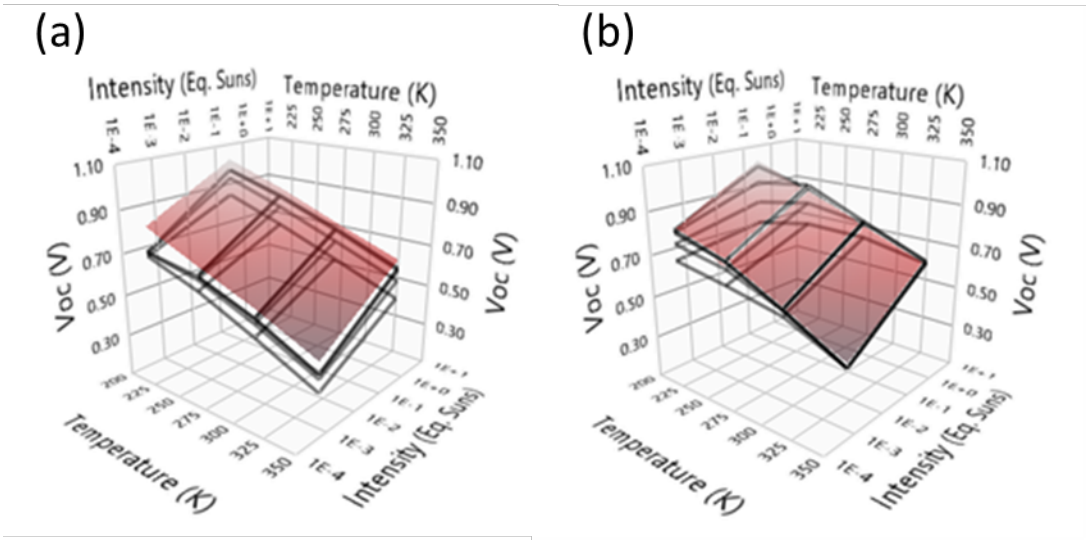


Fig. 4. $V_{OC}$ versus temperature and excitation intensity for the Control sample. $V_{OC}$ data is drawn as a surface, and the grids are simulated $V_{OC}$ values, with parameters varying as: (a) $\Delta E_C$ is changed from 0 to -0.1 to -0.2 to -0.3 eV, making it more cliff-like. Also, $c_s$ was inflated by a factor of 10,000x in these simulations, which is essentially setting an infinite recombination velocity at the interface. (b) $\Delta E_C$ is changed from 0 to +0.1 to +0.2 to +0.3 eV, making it more spike-like. Each parameter step (for both $c_s$ and $\Delta E_C$) corresponds to a grid with a lower $V_{OC}$ .

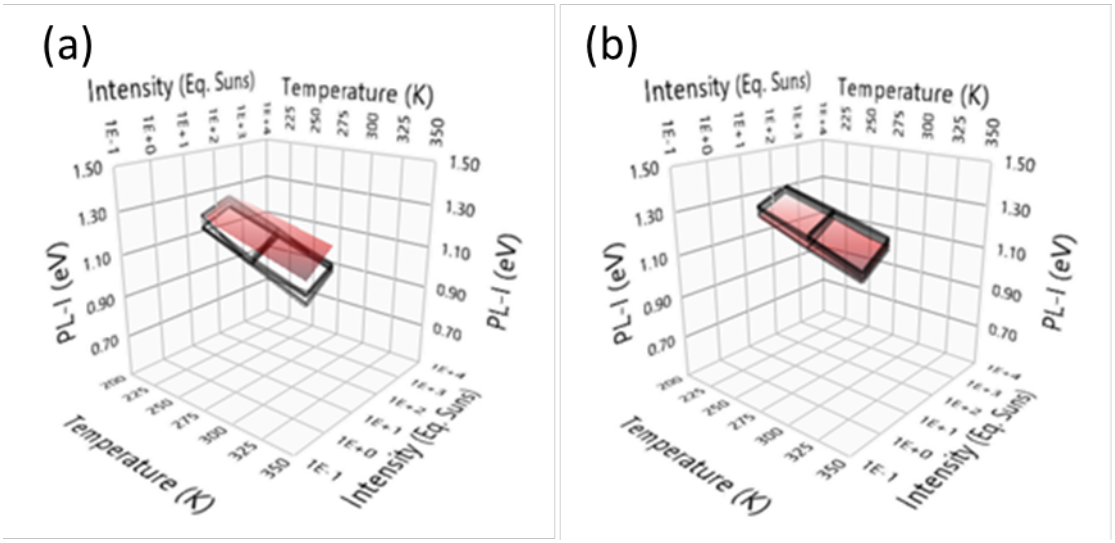


Fig. 5. PL-I versus temperature and excitation intensity. Experimental PL-I data is drawn as a surface, and the grids are simulated PL-I values, with parameters varying as: (a) $\Delta E_C$ is changed from 0 to -0.1 to -0.2 to -0.3 eV, making it more cliff-like. Also, $c_s$ was inflated by a factor of 10,000x in these simulations, which is essentially setting an infinite recombination velocity at the interface. (b) $\Delta E_C$ is changed from 0 to +0.1 to +0.2 to +0.3 eV, making it more spike-like. Each parameter step (for both $c_s$ and $\Delta E_C$) corresponds to a grid with a lower PL-I.

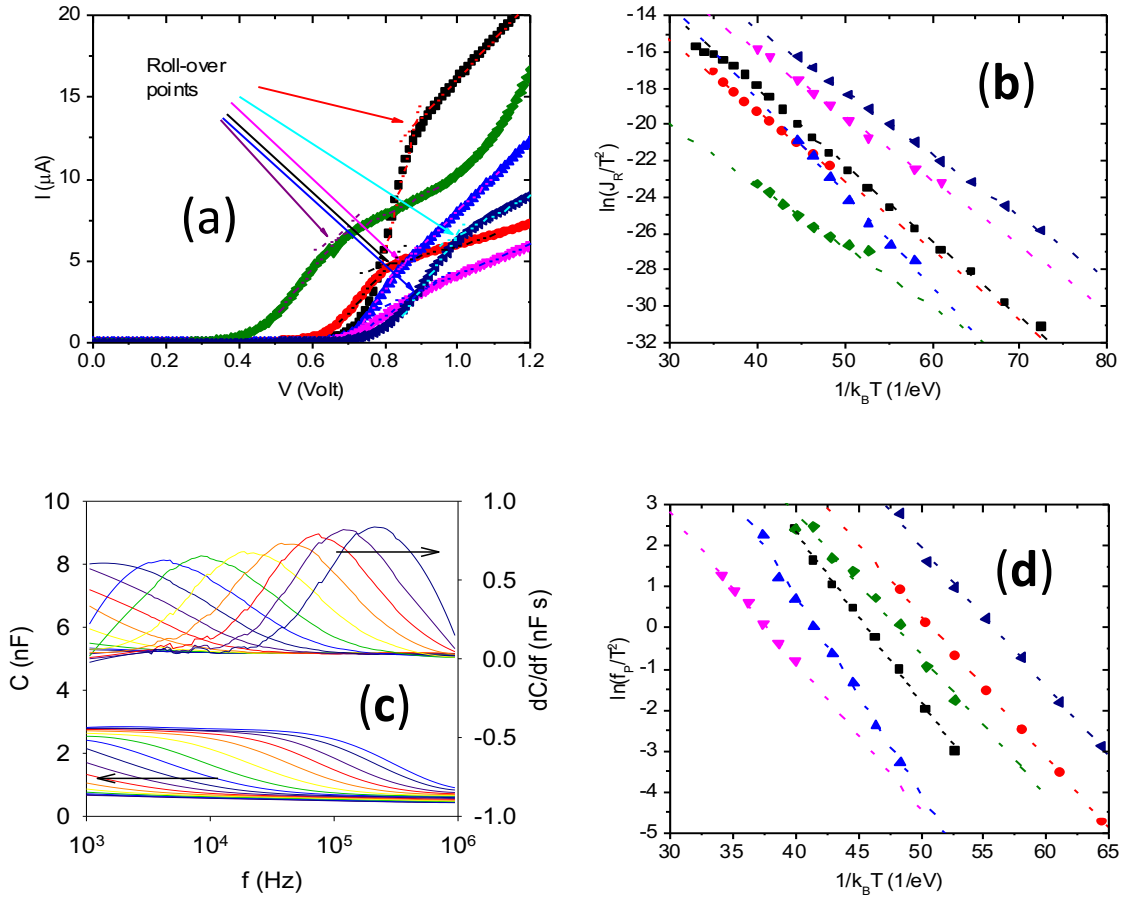


Fig. 6. Comparison of JV-based and capacitance-based methods for measuring back contact offset. Results from the CdS:O[6] samples in Table 1 are shown for illustration. (a) The current of the roll-over point of a JV curve, here shown at 190K, was found as a function of temperature and placed on (b) an Arrhenius plot whose slope provides the barrier height energy. (c) The frequency of the inflection point of an admittance curve was found as a function of temperature and placed on (d) an Arrhenius plot whose slope provides the AS value of barrier height energy.

Results used to extract $\Phi_b$ are shown in Fig. 6. In all cases, the $\Phi_b$ from the JVT rollover effect was 1.1-1.3 times the value from AS, as expected from previous reports. (Li et al., 2010)

The resulting fitted parameters can be seen in Table I, along with $\Phi_b$ and the PCE under AM1.5 solar illumination. The first device on the list is considered the Control sample. A dozen devices were made with the blade-coated CdTe nanoparticle (NP) layer and a dozen without. NP was found to assist in reproducibility, with the best non-NP devices equivalent to the Control device.

We found that lowering the deposition oxygen ratio of CdS:O from 6% to 1% resulted in a more cliff-like $\Delta E_C$ ($< 0$), as might be expected from a decrease in band gap.(Kephart et al., 2015) Although, other studies involving a more drastic lowering of oxygen content have suggested that it could instead increase the band gap by decreasing S-Te diffusion. (Meysing et al., 2016) The

complete substitution of the CdS:O (and undoped $SnO_2$) buffer with a MgZnO buffer causes a strongly spike-like offset ($\Delta E_C > 0$). This is clear from Fig. 7, which develops the same temperature peak seen in Fig. 4 (b).

The bulk recombination coefficient $c_a$ varied from 1-5×$10^7$ $s^{-1}$, with the exception of the final MgZnO device where the $CdCl_2$ activation step took place in an O-free ambient (He gas). The PCE increased from 14 to 15%, and this was attributed to a reduced $c_a$ = 5×$10^6$ $s^{-1}$.

The interfacial recombination coefficient $c_s$ varied from $10^4$ to $10^6$ cm $s^{-1}$. Measurements were sensitive to the value of $c_s$ primarily for the two CdS:O[1] samples (3×$10^5$ cm $s^{-1}$) as these had a cliff-like $\Delta E_C$, making the interface a dominant source of recombination. Thus, this analysis allows the detection of the band alignment as the reason for MZO's success as a front interface contact. In comparison to CdS:O the surface recombination velocity is unimproved or even inferior.

| Device structure starting with glass/$SnO_2$:F/ | PCE | $\Delta Ec$ | $c_a$ | $c_s$ | $\Phi_b$ | $K$ | d$J$/d$V$ |
|---|---|---|---|---|---|---|---|
| | % | eV | $10^7$ $s^{-1}$ | $10^5$ cm $s^{-1}$ | eV | $10^{-5}$ $(\Omega\ V\ cm^2)^{-1}$ | $10^{-5}$ $(\Omega\ cm^2)^{-1}$ |
| $SnO_2$/CdS:O[6]/CdTe/NP/Au | 16 | 0.01 | 1.3 | 0.3 | 0.38 | 4.3 | 29 |
| $SnO_2$/CdS:O[6]/CdTe/NP/ITO/Au | 14.7 | -0.01 | 1.3 | 0.5 | 0.45 | 1.0 | 38 |
| $SnO_2$/CdS:O[6]/CdTe/NP/Se/Au | 15.6 | 0.04 | 3.4 | 0.3 | 0.36 | 6.0 | 86 |
| $SnO_2$/CdS:O[6]/CdTe/NP/SnTe/Au | 13.5 | 0.05 | 1.5 | 0.1 | 0.59 | 0.8 | 21 |
| $SnO_2$/CdS:O[6]/CdTe/NP/Spiro/Au | 10.9 | 0.07 | 5.7 | 1.0 | 0.4 | 5.3 | 130 |
| $SnO_2$/CdS:O[6]/CdTe/NP/EH44/Au | 15 | 0.01 | 2.0 | 0.2 | 0.38 | 5.5 | 100 |
| $SnO_2$/CdS:O[1]/CdTe/Au | 13 | -0.16 | 4.7 | 2.9 | 0.45 | 4.1 | 74 |
| $SnO_2$/CdS:O[1]/CdTe/HI etch/Au | 15 | -0.18 | 2.4 | 3.8 | 0.35 | 4.1 | 46 |
| MgZnO/CdTe/Au | 14 | 0.20 | 2.5 | 11 | 0.38 | 0.1 | 100 |
| MgZnO/CdTe/O-free activ./Au | 15 | 0.22 | 0.5 | 8.0 | 0.38 | 0.1 | 110 |

Table I. Fitting results, with power conversion efficiency, rollover-based barrier height, and slope of the JV curve at the short circuit point.

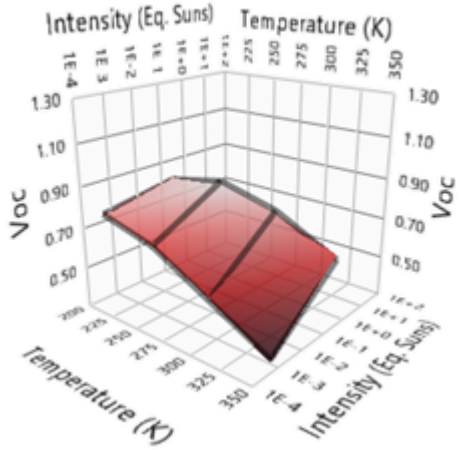


Fig. 7. $V_{OC}$ data (surface) and simulated (mesh) for the MgZnO/CdTe/oxygen-free activated/Au device, illustrating the existence of a spike-like absorber-buffer conduction band offset.

None of the back-contact interlayers was found to make a major reduction of $\Phi_b$, though a hydroiodic (HI) acid etch had reduced the barrier by 0.1 eV below an untreated back surface. What variation in $\Phi_b$ the interlayers caused did not correlate to changes in PCE. In the case of a Se interlayer, for example, the barrier was slightly decreased while the efficiency fell. One interpretation relies on problems in specifying the measured $\Phi_b$ due to inhomogeneous back contact barrier. That is, certain regions of each back contact might have a lower or higher $\Phi_b$ due to local variations in composition. The effective barrier of $\Phi_b^*$ would then be dominated by the lower barrier regions, leading to a temperature-dependent value of $\Phi_b^* \approx \Phi_b - s^2/(2\ k_B T)$ where $s$ is the standard deviation of the barrier height. (Tung, 1991; Werner and Güttler, 1991) The same interpretation was previously suggested when it was found that the amount of $p$-type doping from Cu incorporation was unable to explain the beneficial effect of Cu on the back surface.(Klein, 2015; Perrenoud et al., 2013)

However, the rollover measurements were made in the range 180 K to 280 K. Thus, for the measured rollover $\Phi_b$ to differ appreciably from the room temperature $\Phi_b$, the standard deviation $s$ would need to be very large, yet there is no evidence of a strong quadratic dependence of rollover on reciprocal temperature, nor do previous estimates show a drastic change in $\Phi_b$ at such a temperature range in CdTe devices. (Fiat et al., 2012)

Another cause of PCE variation would be shunting at the front junction. One standard method of estimating shunt conductance is from the derivative d$J$ / d$V$ at the short circuit (zero voltage) point. (Bosio et al., 2018; Ruschel et al., 2016) However, the apparent shunt found from a JV curve is distorted by voltage-dependent collection current and also by the band offsets in heterojunction solar cells. Even when ignoring the effects of $\Phi_b$, this derivative can have an extremely strong dependence on the value of the front band offset $\Delta E_C$. (Li et al., 2018; Sun et al., 2016) The $V_{OC}$-T-I and PL-I-T technique allows an estimation of physical shunting conductance, rather than the lumped parameter of d$J$ / d$V$. Since a device's normal operating

range is ~0.9 Volts, the SCLC shunt conductance constant $K$ in $(\Omega\ V\ cm^2)^{-1}$ may be compared directly to the slope in $(\Omega\ cm^2)^{-1}$ shown Table I, and the shunting is found be an order of magnitude weaker than the slope method would suggest. Most strikingly, the MZO windows yield the worst apparent shunt ($dJ / dV$) yet the best shunt from the fitted VOC-T-I & PL-I-T data.

That the slope method gives an inaccurate value is clear from the low intensity $V_{OC}$, where the device is simply not being provided with enough photocurrent to account for an Ohmic shunt of conductance $dJ / dV$. This suggests that the many reported estimations of shunting by the standard slope method largely do not represent a physically meaningful shunting path in heterojunction solar cells. Shunt resistances estimated by the slope method must not be taken as representing a physical shunting connection unless they are far below 1 $k\Omega\ cm^2$.

One result which does not appear in the Table is that of the PbTe:Tl interlayered device. This device was unusual because there is no rollover, and hence no evidence of $\Phi_b$ in the JV curve shown in Fig. 8. We include the Control device, for direct comparison, which shows the rollover near 1 V. Moreover, the PbTe:Tl device's C-V results, shown in Fig. 9 as a Mott plot, $N_{CV} = (2/q\varepsilon)/[d(C^{-2})/dV]$, do not show the U-shape expected for structures with a back contact barrier,(Li et al., 2012) as seen on the Control sample's C-V result which is representative of all of the other devices.

It is possible that the lack of a U-shaped C-V result could be related to a Cu diffusion effect seen in previously reported C-V results that were similar in appearance and depth.(Boucher et al., 2014; Rimmaudo et al., 2017) But, in the present case, the Cu was already deposited and diffused before the PbTe interlayer, and even the sample with a SnTe interlayer did not exhibit these effects despite undergoing a close to identical process. The time-resolved photoluminescence (TRPL) lifetime was the highest for the PbTe device as well. (Details to be published later by S. Rab, *et. al.*) All of these suggest that PbTe:Tl is forming an excellent Ohmic contact.

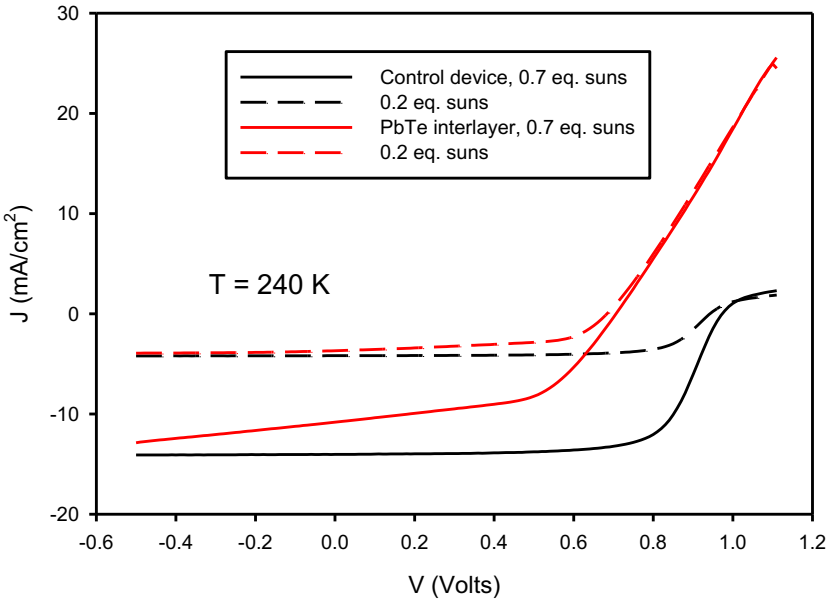

Fig. 8. Comparison of typical JV curves the with those from the PbTe:Tl back contact interlayer device.

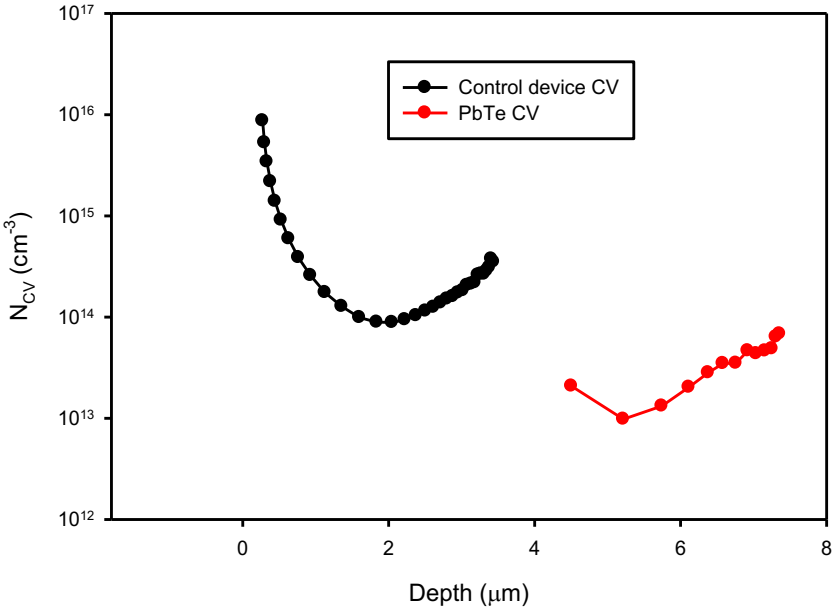


Fig. 9. Room temperature comparison of typical C-V effective doping concentration curves with those of the PbTe:Tl back contact interlayer device.

However, this device has the lowest efficiency of all (9%) with a $V_{OC}$ that does not rise above 700 mV. We believe that there is an additional presence of a strong photoconducting shunt, caused by the PbTe interlayer. The effect can be seen on the more strongly illuminated JV curves in Fig. 8. While the slope method is not normally quantitative, the overall linear form of the JV curve suggests a very high shunt of 200 Ω $cm^2$, but only when illuminated. It appears that the interface between PbTe and CdTe is undergoes complicated changes in band bending with light, which is not unexpected from previous studies of strong band-bending and persistent photoconductivity when these materials are grown together in single crystal form. (Swartz et al., 2016; Zhang et al., 2014)

## 5. Conclusions

In summary, the back-contact barrier and the front buffer conduction band offset present special challenges for heterojunction solar cells such as those based on CdTe. Not only do they impact cell performance, but methods for their characterization are still unsettled. Further, they compound the difficulty of characterizing more conventional obstacles such as recombination centers and shunting. $V_{OC}$-T-I allows a certain amount of insight, associating clear, measurable features with the desired offsets and shunts. When complemented with PL-I-T, signatures of band offsets which are otherwise difficult to distinguish from recombination effects become more resolvable. With numerical simulation, the recombination characteristics, offsets, and shunts can be obtained quantitatively.

ITO and SnTe:Tl interlayers were successful at reducing shunt, but the barrier height did not show the hoped-for reduction. The other interlayers attempted did not significantly reduce the shunt or barrier, though HI etching reduced the back-barrier height by 0.1 eV in CdS:$O^-$ samples suggesting that a direct reduction in $\Phi_b$, rather than a Cu diffusion reduction mechanism, is responsible for the improved performance of a Te-rich surface. Heavily Tl doped PbTe appeared to reduce or eliminate the barrier height, yet it was marred by strongly photoconducting shunt. This suggests a possibility that *p*-PbTe, in combination with another interlayer, may eliminate the shunt effect while lowering the barrier.

The doping of CdS with oxygen to widen the band gap appears to have effect of raising its conduction band with respect to CdTe, yielding a less cliff-like offset. The increasingly popular MgZnO (MZO) front buffer has a large spike-like offset which effectively reduces interfacial recombination without reducing recombination velocity, and tuning the Mg/Zn ratio to obtain a reduction in gap of 0.1 eV may prove beneficial.

## 6. Acknowledgments

This work was authored in part by the National Renewable Energy Laboratory, operated by Alliance for Sustainable Energy, LLC, for the U.S. Department of Energy (DOE) under Contract No. DE-AC36-08GO28308. This material is based upon the work supported by the U.S. Department of Energy's Office of Energy Efficiency and Renewable Energy (EERE) under Solar Energy Technologies Office (SETO) Agreement Number DE-EE0007541. Devices were grown during work supported by the U.S. Department of Energy's NREL under (SuNLaMP) - "Interface Science and Engineering for Reliable, High Efficiency CdTe". J.V. Li acknowledges current funding from Ministry of Science and Technology, Taiwan, under grant number MOST 107-2218-E-006-022-MY3. The authors would like to thank the Sellinger group at the Colorado School of Mines for providing the EH44 used. The views expressed in the article do not necessarily represent the views of the DOE or the U.S. Government. The U.S. Government retains and the publisher, by accepting the article for publication, acknowledges that the U.S. Government retains a nonexclusive, paid-up, irrevocable, worldwide license to publish or reproduce the published form of this work, or allow others to do so, for U.S. Government purposes.

Böer, K.W., 2013 Handbook of the Physics of Thin-Film Solar Cells Springer, Berlin, Germany.
Bosio, A., Ciprian, R., Lamperti, A., Rago, I., Ressel, B., Rosa, G., Stupar, M., Weschke, E., 2018. Interface phenomena between CdTe and ZnTe:Cu back contact. Solar Energy 176, 186-193.
Boucher, J.W., Miller, D.W., Warren, C.W., Cohen, J.D., McCandless, B.E., Heath, J.T., Lonergan, M.C., Boettcher, S.W., 2014. Optical response of deep defects as revealed by transient photocapacitance and photocurrent spectroscopy in CdTe/CdS solar cells. Sol. Energy Mater. Sol. Cells 129, 57-63.
Brandt, R.E., Mangan, N.M., Li, J.V., Lee, Y.S., Buonassisi, T., 2017. Determining interface properties limiting open-circuit voltage in heterojunction solar cells. J. Appl. Phys. 121(18), 185301.
Chan, D.S.H., Phillips, J.R., Phang, J.C.H., 1986. A comparative study of extraction methods for solar cell model parameters. Solid·State Electron. 29(3), 329-337.

Demtsu, S.H., Albin, D.S., Pankow, J.W., Davies, A., 2006. Stability study of CdS/CdTe solar cells made with Ag and Ni back-contacts. Sol. Energy Mater. Sol. Cells 90(17), 2934-2943.
Dongaonkar, S., Servaites, J.D., Ford, G.M., Loser, S., Moore, J., Gelfand, R.M., Mohseni, H., Hillhouse, H.W., Agrawal, R., Ratner, M.A., Marks, T.J., Lundstrom, M.S., Alam, M.A., 2010. Universality of non-Ohmic shunt leakage in thin-film solar cells. J. Appl. Phys. 108(12), 124509.
Fiat, S., Merdan, Z., Memmedli, T., 2012. Current-conduction mechanisms in Au/n-CdTe Schottky solar cells in the wide temperature range. Physica B: Condensed Matter 407(13), 2560-2565.
Gloeckler, M., Fahrenbruch, A.L., Sites, J.R., 2003. Numerical modeling of CIGS and CdTe solar cells: setting the baseline, Proceedings of 3rd World Conference on Photovoltaic Energy Conversion. IEEE, Osaka, Japan, pp. 491-494.
Grover, S., Li, J.V., Young, D.L., Stradins, P., Branz, H.M., 2013. Reformulation of solar cell physics to facilitate experimental separation of recombination pathways. Appl. Phys. Lett. 103(9), 093502.
Guo, H., Andagana, H.B., Cao, X.A., 2010. Au-Doped Indium Tin Oxide Ohmic Contacts to p-Type GaN. J. Electron. Mater. 39(5), 494-498.
Halverson, A., Yakimov, A., Vert, A., Sulima, O., Korevaar, B., 2013. Side-by-side characterization of non-optimized and optimized CdS/CdTe solar cells on commercial transparent conductive oxide/glass. Thin Solid Films 535, 249-252.
Hegedus, S.S., Shafarman, W.N., 2004. Thin-film solar cells: device measurements and analysis. Prog. Photovoltaics Res. Appl. 12(2-3), 155-176.
Helander, M.G., Greiner, M.T., Wang, Z.B., Tang, W.M., Lu, Z.H., 2011a. Work function of fluorine doped tin oxide. Journal of Vacuum Science & Technology A 29(1), 011019.
Helander, M.G., Wang, Z.B., Qiu, J., Greiner, M.T., Puzzo, D.P., Liu, Z.W., Lu, Z.H., 2011b. Chlorinated Indium Tin Oxide Electrodes with High Work Function for Organic Device Compatibility. Science 332(6032), 944-947.
Jaegermann, W., Klein, A., Mayer, T., 2009. Interface Engineering of Inorganic Thin-Film Solar Cells – Materials-Science Challenges for Advanced Physical Concepts. Advanced Materials 21(42), 4196-4206.
Jordehi, A.R., 2016. Parameter estimation of solar photovoltaic (PV) cells: A review. Renewable and Sustainable Energy Reviews 61, 354-371.
Kephart, J.M., Geisthardt, R.M., Sampath, W.S., 2015. Optimization of CdTe thin-film solar cell efficiency using a sputtered, oxygenated CdS window layer. Prog. Photovoltaics Res. Appl. 23(11), 1484-1492.
Khan, F., Singh, S.N., Husain, M., 2011. Determination of the diode parameters of a-Si and CdTe solar modules using variation of the intensity of illumination: An application. Solar Energy 85(9), 2288-2294.
Klein, A., 2015. Energy band alignment in chalcogenide thin film solar cells from photoelectron spectroscopy. Journal of Physics: Condensed Matter 27(13), 134201.
Koishiyev, G.T., Sites, J.R., Kulkarni, S.S., Dhere, N.G., 2008. Determination of back contact barrier height in Cu(In,Ga)(Se,S)2 and CdTe solar cells, 2008 33rd IEEE Photovoltaic Specialists Conference. pp. 1-3.
Korevaar, B.A., Shuba, R., Yakimov, A., Cao, H., Rojo, J.C., Tolliver, T.R., 2011. Initial and degraded performance of thin film CdTe solar cell devices as a function of copper at the back contact. Thin Solid Films 519(21), 7160-7163.
Lauwaert, J., Van Puyvelde, L., Lauwaert, J., Thybaut, J.W., Khelifi, S., Burgelman, M., Pianezzi, F., Tiwari, A.N., Vrielinck, H., 2013. Assignment of capacitance spectroscopy signals of CIGS solar cells to effects of non-ohmic contacts. Sol. Energy Mater. Sol. Cells 112, 78-83.
Lee, K.-K., Priyantha, W., Myers, T.H., 2012. Growth and valence band offset measurement of PbTe/InSb heterojunctions. Appl. Phys. Lett. 100(5), 052108.
Leijtens, T., Giovenzana, T., Habisreutinger, S.N., Tinkham, J.S., Noel, N.K., Kamino, B.A., Sadoughi, G., Sellinger, A., Snaith, H.J., 2016. Hydrophobic Organic Hole Transporters for Improved Moisture Resistance in Metal Halide Perovskite Solar Cells. ACS Applied Materials & Interfaces 8(9), 5981-5989.

Li, J.V., Grover, S., Contreras, M.A., Ramanathan, K., Kuciauskas, D., Noufi, R., 2014. A recombination analysis of Cu(In,Ga)Se2 solar cells with low and high Ga compositions. Sol. Energy Mater. Sol. Cells 124, 143-149.
Li, J.V., Halverson, A.F., Sulima, O.V., Bansal, S., Burst, J.M., Barnes, T.M., Gessert, T.A., Levi, D.H., 2012. Theoretical analysis of effects of deep level, back contact, and absorber thickness on capacitance–voltage profiling of CdTe thin-film solar cells. Sol. Energy Mater. Sol. Cells 100, 126-131.
Li, J.V., Johnston, S.W., Li, X., Albin, D.S., Gessert, T.A., Levi, D.H., 2010. Discussion of some "trap signatures" observed by admittance spectroscopy in CdTe thin-film solar cells. J. Appl. Phys. 108(6), 064501.
Li, X., Shen, K., Li, Q., Deng, Y., Zhu, P., Wang, D., 2018. Roll-over behavior in current-voltage curve introduced by an energy barrier at the front contact in thin film CdTe solar cell. Solar Energy 165, 27-34.
López Salas, J.F., Richter, M., Parisi, J., Heise, S.J., 2017. Simulation of photoluminescence lifetime and open-circuit voltage in Cu(In,Ga)Se2 thin film solar cells. J. Appl. Phys. 122(20), 203103.
Major, J.D., Phillips, L.J., Al Turkestani, M., Bowen, L., Whittles, T.J., Dhanak, V.R., Durose, K., 2017. P3HT as a pinhole blocking back contact for CdTe thin film solar cells. Sol. Energy Mater. Sol. Cells 172, 1-10.
Mangan, N.M., Brandt, R.E., Steinmann, V., Jaramillo, R., Yang, C., Poindexter, J.R., Chakraborty, R., Park, H.H., Zhao, X., Gordon, R.G., Buonassisi, T., 2015. Framework to predict optimal buffer layer pairing for thin film solar cell absorbers: A case study for tin sulfide/zinc oxysulfide. J. Appl. Phys. 118(11), 115102.
Marin, A.T., Musselman, K.P., MacManus-Driscoll, J.L., 2013. Accurate determination of interface trap state parameters by admittance spectroscopy in the presence of a Schottky barrier contact: Application to ZnO-based solar cells. J. Appl. Phys. 113(14), 144502.
Meysing, D.M., Reese, M.O., Warren, C.W., Abbas, A., Burst, J.M., Mahabaduge, H.P., Metzger, W.K., Walls, J.M., Lonergan, M.C., Barnes, T.M., Wolden, C.A., 2016. Evolution of oxygenated cadmium sulfide (CdS:O) during high-temperature CdTe solar cell fabrication. Sol. Energy Mater. Sol. Cells 157, 276-285.
Ott, T., Schönberger, F., Walter, T., Hariskos, D., Kiowski, O., Salomon, O., Schäffler, R., 2015. Verification of phototransistor model for Cu(In,Ga)Se2 solar cells. Thin Solid Films 582, 392-396.
Pan, J., Gloeckler, M., Sites, J.R., 2006. Hole current impedance and electron current enhancement by back-contact barriers in CdTe thin film solar cells. J. Appl. Phys. 100(12), 124505.
Passlack, M., Legge, R.N., Convey, D., Yu, Z.Y., Abrokwah, J.K., 1998. Optical measurement system for characterizing compound semiconductor interface and surface states. IEEE Trans. Instrum. Meas. 47(5), 1362-1366.
Perrenoud, J., Kranz, L., Gretener, C., Pianezzi, F., Nishiwaki, S., Buecheler, S., Tiwari, A.N., 2013. A comprehensive picture of Cu doping in CdTe solar cells. J. Appl. Phys. 114(17), 174505.
Proctor, C.M., Nguyen, T.-Q., 2015. Effect of leakage current and shunt resistance on the light intensity dependence of organic solar cells. Appl. Phys. Lett. 106(8), 083301.
Richter, M., Schubbert, C., Eraerds, P., Parisi, J., Riedel, I., Dalibor, T., Palm, J., 2015. Comprehensive simulation model for Cu(In,Ga)(Se,S)2 solar cells. Sol. Energy Mater. Sol. Cells 132, 162-171.
Rimmaudo, I., Salavei, A., Artegiani, E., Menossi, D., Giarola, M., Mariotto, G., Gasparotto, A., Romeo, A., 2017. Improved stability of CdTe solar cells by absorber surface etching. Sol. Energy Mater. Sol. Cells 162, 127-133.
Ruschel, C.S., Gasparin, F.P., Costa, E.R., Krenzinger, A., 2016. Assessment of PV modules shunt resistance dependence on solar irradiance. Solar Energy 133, 35-43.
Schoneberg, J., Ohland, J., Eraerds, P., Dalibor, T., Parisi, J., Richter, M., 2018. Accessing the band alignment in high efficiency Cu(In,Ga)(Se,S)2 (CIGSSe) solar cells with an InxSy:Na buffer based on temperature dependent measurements and simulations. J. Appl. Phys. 123(15), 155701.
Schubbert, C., Eraerds, P., Richter, M., Parisi, J., Riedel, I., Dalibor, T., Palm, J., 2015. Anomalous temperature dependence of the open-circuit voltage of InS-buffered Cu(In,Ga)(Se,S) solar cells simulated in broad temperature range. physica status solidi (a) 213(5), 1276-1283.

Seidman, T.I., Choo, S.C., 1972. Iterative scheme for computer simulation of semiconductor devices. Solid·State Electron. 15(11), 1229-1235.
Sohal, S., Edirisooriya, M., Myers, T., Holtz, M., 2018. Investigation of cadmium telluride grown by molecular-beam epitaxy using micro-Raman spectroscopy below and above the laser damage threshold. J. Vac. Sci. Technol. B 36(5), 052905.
Song, T., Kanevce, A., Sites, J.R., 2016. Emitter/absorber interface of CdTe solar cells. J. Appl. Phys. 119(23), 233104.
Song, T., Moore, A., Sites, J.R., 2018. Te Layer to Reduce the CdTe Back-Contact Barrier. IEEE J. Photovolt. 8(1), 293-298.
Sozzi, G., Troni, F., Menozzi, R., 2014. On the combined effects of window/buffer and buffer/absorber conduction-band offsets, buffer thickness and doping on thin-film solar cell performance. Sol. Energy Mater. Sol. Cells 121, 126-136.
Storn, R., Price, K., 1997. Differential Evolution – A Simple and Efficient Heuristic for global Optimization over Continuous Spaces. Journal of Global Optimization 11(4), 341-359.
Sun, X., Silverman, T., Garris, R., Deline, C., Alam, M.A., 2016. An Illumination- and Temperature-Dependent Analytical Model for Copper Indium Gallium Diselenide (CIGS) Solar Cells. IEEE J. Photovolt. 6(5), 1298-1307.
Swartz, C.H., Paul, S., Mansfield, L.M., Holtz, M.W., 2019. Absolute photoluminescence intensity in thin film solar cells. J. Appl. Phys. 125(5), 053103.
Swartz, C.H., Petersen, J.E., Welch, E.W., Myers, T.H., 2016. The Effect of Anisotropic Valleys on Phonon Scattering and the Magnetotransport Properties of n-Type PbTe. J. Electron. Mater. 45(1), 722-728.
Tessema, M.M., Giolando, D.M., 2012. Pinhole treatment of a CdTe photovoltaic device by electrochemical polymerization technique. Sol. Energy Mater. Sol. Cells 107, 9-12.
Tung, R.T., 1991. Electron transport of inhomogeneous Schottky barriers. Appl. Phys. Lett. 58(24), 2821-2823.
Turek, M., 2014. Current and illumination dependent series resistance of solar cells. J. Appl. Phys. 115(14), 144503.
Wang, T., Du, S., Li, W., Liu, C., Zhang, J., Wu, L., Li, B., Zeng, G., 2017. Control of Cu doping and CdTe/Te interface modification for CdTe solar cells. Materials Science in Semiconductor Processing 72, 46-51.
Werner, J.H., Güttler, H.H., 1991. Barrier inhomogeneities at Schottky contacts. J. Appl. Phys. 69(3), 1522-1533.
Xia, W., Lin, H., Wu, H.N., Tang, C.W., Irfan, I., Wang, C., Gao, Y., 2014. Te/Cu bi-layer: A low-resistance back contact buffer for thin film CdS/CdTe solar cells. Sol. Energy Mater. Sol. Cells 128, 411-420.
Zhang, B., Cai, C., Zhu, H., Wu, F., Ye, Z., Chen, Y., Li, R., Kong, W., Wu, H., 2014. Phonon blocking by two dimensional electron gas in polar CdTe/PbTe heterojunctions. Appl. Phys. Lett. 104(16), 161601.